

and Kirby<sup>39</sup> for phosphate ( $-P(O)(OR)_2$ ) transfer, by the weak bonding between entering and leaving groups and the sulfur in the controlling transition state.

**Acknowledgment.** We are grateful to the SERC and to ICI Organics Division for financial support and to Dr. P. Bamfield for his helpful advice.

**Registry No.** 14-K (Ar = Ph), 1733-88-6; 14-K (Ar = 3,4-(NO<sub>2</sub>)<sub>2</sub>C<sub>6</sub>H<sub>3</sub>), 86260-33-5; 14-K (Ar = 2,6-(NO<sub>2</sub>)<sub>2</sub>C<sub>6</sub>H<sub>3</sub>), 86260-34-6; 14-K (Ar = 2,3-(NO<sub>2</sub>)<sub>2</sub>C<sub>6</sub>H<sub>3</sub>), 86260-35-7; 14-K (Ar = 2,4-(NO<sub>2</sub>)<sub>2</sub>C<sub>6</sub>H<sub>3</sub>), 72119-41-6; 14-K (Ar = 4-Cl, 2-NO<sub>2</sub>C<sub>6</sub>H<sub>3</sub>), 86260-36-8;

14-K (Ar = 2-Cl, 4-NO<sub>2</sub>C<sub>6</sub>H<sub>3</sub>), 86260-37-9; 15 (X = H), 42824-16-8; 15 (X = 3-Me), 55546-46-8; 15 (X = 4-Me), 86260-30-2; 15 (X = 3,4-(Me)<sub>2</sub>), 86260-31-3; 15 (X = 3,5-(Me)<sub>2</sub>), 86260-32-4; TEA, 102-71-6; DABCO, 280-57-9; isoquinolium-*N*-sulfate, 53854-50-5; phenoxide, 3229-70-7; 3,5-dimethylphenoxide, 67303-73-5; 2,5-dimethylphenoxide, 64502-87-0; 2,4-dimethylphenoxide, 86260-38-0; 3-chlorophenoxide, 18938-14-2; 2,3-dimethylphenoxide, 86260-39-1; 4-chlorophenoxide, 24573-38-4; 2,6-dimethylphenoxide, 25117-01-5; 3-methylphenoxide, 20227-79-6; ethyl glycinate, 459-73-4; glycine, 56-40-6; ethanolamine, 141-43-5; *n*-propylamine, 107-10-8; methyl  $\beta$ -alaninate, 4138-35-6; aminoacetonitrile, 540-61-4; diaminoethane, 107-15-3; semicarbazide, 57-56-7; aniline, 62-53-3; hydrazine, 302-01-2; *N*-ethylmorpholine, 100-74-3; *N,N*-diethanolamine, 111-42-2; triethylamine, 121-44-8; trimethylamine, 75-50-3; *N*-methylpiperidine, 626-67-5; acetate anion, 71-50-1; phosphate dianion, 14066-19-4; carbonate dianion, 3812-32-6; cacodylate, 15132-04-4; water, 7732-18-5; hydroxide ion, 14280-30-9.

(39) Khan, S. A.; Kirby, A. J. *J. Chem. Soc. B* 1970, 1172.

## Phase Separation and Reactivity Changes of Phenyl Ester Substrate and Imidazole Catalyst in the Dialkylammonium Bilayer Membrane

Toyoki Kunitake,\* Hirotaka Ihara, and Yoshio Okahata

Contribution No. 666 from the Department of Organic Synthesis, Faculty of Engineering, Kyushu University, Fukuoka 812, Japan. Received October 4, 1982.  
Revised Manuscript Received May 17, 1983

**Abstract:** A phenyl ester substrate and an imidazole catalyst that possess the azobenzene chromophore and are capable of bilayer formation were synthesized. Distribution of these amphiphiles in the dialkylammonium bilayer matrix was examined by using blue shifts due to cluster formation of the azobenzene chromophore. Formation of the substrate cluster was promoted by increased concentrations in the matrix and by the liquid crystal-to-crystal phase transition of the matrix. Formation of the catalyst cluster was promoted, in addition to these factors, by neutralization of the anionic histidine head group due to the change of the medium pH or due to complexation with Cu<sup>2+</sup> ion. The rate of alkaline hydrolysis of the clustered substrate was smaller than that of the isolated (monomeric) substrate:  $1/19$  at 10 °C, pH 11.8. The Arrhenius plots show inflection regions near the phase transition of the matrix due to changing monomer-cluster ratios. The activation energy of the hydrolysis of *p*-nitrophenyl *N*-carbobenzoxy-L-phenylalaninate was 27 kcal/mol in the partially rigid bilayer matrix but decreased to 14 kcal/mol in the fluid matrix. This change was attributed to the formation of the catalyst cluster in the rigid matrix. The present study provides the first example of the reaction control by phase separation.

The physiological function of the biomembrane is closely related to the mode of distribution and the corresponding activity change of membrane enzymes.<sup>1-6</sup> In spite of the overriding physiological importance of the regulation of activity of these enzymes, its molecular understanding is lagging because of the inherent difficulty arising from the complexity of the system. Thus, the molecular mechanism of regulation may be tested more readily by using simplified, synthetic systems.

Our aim in the present series of investigation is to establish the relation between the mode of distribution (phase separation in particular) of reacting species (catalyst, substrate, etc.) and their reactivities in the synthetic bilayer matrix. The relationship, if established, would provide useful information for understanding the mode of action of membrane enzymes and for designing synthetic catalysts with regulatory functions.

Recently, it was shown in these laboratories that phase separation of single-chain ammonium amphiphiles with the azobenzene moiety can be detected spectroscopically.<sup>7</sup> When a sonicated aqueous mixture (molar ratio, 1:10) of azobenzene amphiphile **1** and dialkylammonium amphiphile **5** ( $n = 18$ ) was maintained at 50 °C,  $\lambda_{\max}$  of the azobenzene chromophore appeared at 355 nm, indicating the presence of monomeric azobenzene species. The monomer peak disappeared upon cooling, and a new peak due to the azobenzene cluster appeared at 316 nm. The spectral change was reversible. This finding provides a new, facile technique for detection of phase separation in the synthetic membrane system, and a variety of novel functions are conceivable on the basis of this technique. For instance, phase separation of probe molecules in the bilayer matrix can be regulated by the interaction of the surface receptor (neutral and protonated ethylenediamine moiety) and added ions, and this system can be applied quite generally to detection of chemical signals.<sup>8</sup>

We applied this technique to examine phase separation and the resulting reactivity changes of a phenyl ester substrate and an imidazole catalyst in the dialkylammonium bilayer matrix. Amphiphile **2** was selected as membrane-forming substrate because

(1) McMurchie, E. J.; Raison, J. K. *Biochem. Biophys. Acta* 1979, 554, 364-374.

(2) McMurchie, E. J.; Raison, J. K.; Cairncross, K. D. *Comp. Biochem. Physiol. B* 1973, 44B, 1017-1026.

(3) Raison, J. K.; McMurchie, E. J. *Biochem. Biophys. Acta* 1974, 363, 135-140.

(4) Okuyama, H.; Saito, M.; Joshi, V. C.; Gunsberg, S.; Wakil, S. J. *J. Biol. Chem.* 1979, 254, 12281-12284.

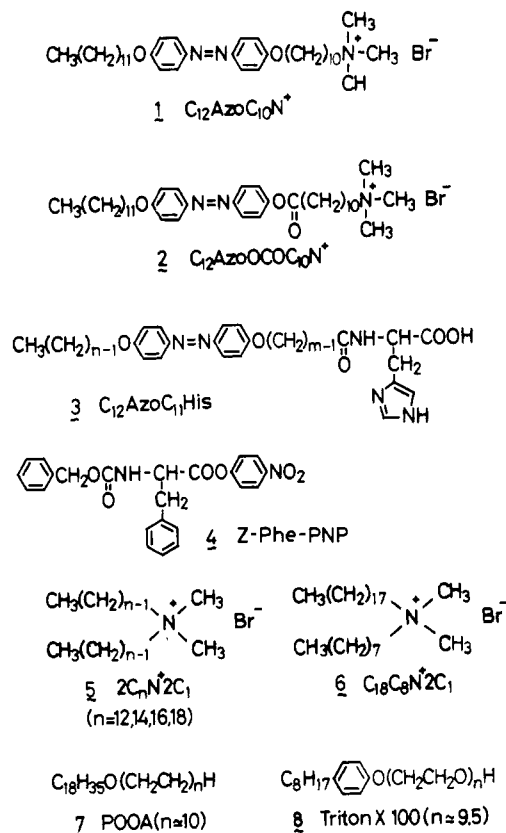
(5) Tanaka, R.; Teruya, A. *Biochem. Biophys. Acta* 1973, 323, 584-591.

(6) Uehara, K.; Akutsu, H.; Kyogoku, Y.; Akamatsu, Y. *Biochem. Biophys. Acta* 1977, 466, 393-401.

(7) Shimomura, M.; Kunitake, T. *Chem. Lett.* 1981, 1001-1004.

(8) Shimomura, M.; Kunitake, T. *J. Am. Chem. Soc.* 1982, 104, 1757-1759.

Chart I



of its structural similarity to probe amphiphile **1**, and its alkaline hydrolysis was studied. In the catalytic hydrolysis, an azobenzene-containing amphiphile that contains the L-histidine head (**3**) was used. A substrate combined with this catalyst was *p*-nitrophenyl *N*-(benzoxycarbonyl)phenylalaninate (**4**), because it shows high reactivity without specific binding to the membrane.

The molecular structure of the reagents and their abbreviations are given in Chart I.

### Experimental Section

**Materials.** The structure and purity of the reaction products were usually confirmed by NMR and IR spectroscopy and thin layer chromatography.

4-[(4-(Dodecyloxy)phenyl)azo]phenol (1.5 g, 4 mmol), mp 104–104.5 °C and 1.1 g (4 mmol) of 11-bromoundecanoic acid were allowed to react in dry tetrahydrofuran (THF) in the presence of 1.0 g (5 mmol) of dicyclohexylcarbodiimide and a small amount of *p*-(dimethylamino)pyridine for 2 days at room temperature. After separation of dicyclohexylurea, 100 mL of methanol was added to the solution to give yellow powdery precipitates: yield 1.8 g (72%); mp 73 → 102 °C (the liquid crystalline region indicated by the arrow). The ester product (1.5 g, 2.4 mmol) was dissolved in a mixture of 50 mL of dry THF and 100 mL of dry benzene, and dry trimethylamine gas was introduced to the solution for 1 h. The mixture was stirred for 6 h at room temperature. The precipitates were washed with ether and recrystallized from a mixture of  $CHCl_3$  and ether to give yellow needles of **2**: yield 1.2 g (74%); mp 140 → 230 °C dec. Anal. Calcd for  $C_{38}H_{62}N_3O_3Br \cdot H_2O$ : C, 64.75; H, 9.15; N, 5.96. Found: C, 64.75; H, 9.07; N, 5.89.

4-[(4-(Dodecyloxy)phenyl)azo]phenol (7.7 g, 20 mmol), 5.5 g (20 mmol) of commercial 11-bromoundecanoic acid, and 3.0 g (44 mmol) of 85% KOH were dissolved in 200 mL of ethanol and the mixture was refluxed for 6 h. Two milliliters of concentrated hydrochloric acid and 30 mL of acetic acid were added to the mixture, which was then heated for 5 min and allowed to cool to room temperature. The precipitates were washed carefully with water, methanol, and ether and recrystallized from a mixture of acetic acid (100 mL) and ethyl acetate (200 mL): yellow flakes; yield 5.3 g (47%); mp 131–132 °C. Completion of the alkylation was confirmed by TLC-FID and IR spectroscopy.

11-(4-((4-(Dodecyloxy)phenyl)azo)phenyloxy)undecanoic acid thus obtained (2.0 g, 3.5 mmol) and 5 g of  $Na_2CO_3$  were heated in 30 mL of refluxing  $SOCl_2$  for 2 h. Excess  $SOCl_2$  was removed in vacuo and the residue extracted with 30 mL of dry benzene. The extract was added

dropwise to a solution of 2.6 g (5 mmol) of the bis(*p*-toluenesulfonate) of L-histidine ethyl ester<sup>9,10</sup> and 2.8 mL (20 mmol) of triethylamine in 20 mL of dry DMF, and the mixture was stirred at room temperature for 2 days. The mixture was made homogeneous by warming, 100 mL of methanol were added, and yellow powders that separated upon ice cooling were washed with methanol, ethanol, and ether: yield 1.7 g (65%); mp 110 → 173 °C. The product, dissolved in hot THF, was mixed with aqueous ethanol containing 1.5 equiv of KOH, and the mixture was heated for 10 min. The precipitates obtained upon cooling were washed with water, methanol, and ether to give the  $C_{12}AzoC_{11}His$  catalyst: yellow powder, mp 203 → 293 °C dec. Anal. Calcd for  $C_{41}H_{60}N_5O_5K \cdot H_2O$ : C, 64.79; H, 8.22; N, 9.22. Found: C, 64.40; H, 8.23; N, 9.00.

The *p*-nitrophenyl ester of *N*-carbobenzoxy-L-phenylalanine, Z-Phe-PNP, was prepared by the procedure of Bodanszky and du Vigneaud.<sup>11</sup> mp 124.5–126.0 °C (lit.<sup>11</sup> 126–126.5 °C). Anal. Calcd for  $C_{23}H_{20}N_2O_6$ : C, 65.71; H, 4.80; N, 6.66. Found: C, 65.61; H, 4.78; N, 6.81. Dialkylammonium bromides, **5** and **6**, were obtained by the stepwise alkylation.<sup>12</sup> Commercial POOA (**7**) and Triton X-100 (**8**) were used as received.

**Spectral Measurement.** In a typical procedure, given amounts of dialkylammonium salts and substrate or catalyst were placed in a vial, and a few milliliters of dilute hydrochloric acid (pH 2–3) were added. The mixture was sonicated with a Bransonic sonifier (microtip, power 40) to give a yellow, clear stock solution. The stock solution (10–100  $\mu$ L) was added to 3400  $\mu$ L of aqueous buffers in quartz cells and subjected to aging for 20–60 min at specified temperatures, and the spectrum was obtained with a Hitachi 124 spectrophotometer. The buffer solutions used are 0.01–0.02 M acetate ( $\mu = 0.02$ ), 0.02 M borate ( $\mu = 0.01$ ), 0.01 N HCl ( $\mu = 0.01$ ), and 0.01 N NaOH ( $\mu = 0.01$ ). The temperature dependence of the absorption spectrum was examined by starting from the high-temperature side. In this case, the solution was aged for 1 h prior to the spectral measurement at the respective temperature.

In the alkaline hydrolysis of **2**, 100  $\mu$ L of the stock solution was injected into 3400  $\mu$ L of borate buffer (0.01–0.02 M,  $\mu = 0.01$  with KCl) that had been maintained at the given temperature ( $\pm 0.1$  °C). The catalyzed hydrolysis was initiated by addition of an acetonitrile solution (20  $\mu$ L) of substrate to an aqueous buffer (3000  $\mu$ L) containing given concentrations of catalyst and matrix membrane. The hydrolysis process was followed by determining the absorbance change of the phenolate anion at 390–420 nm.

**Other Measurements.** The pH value was determined with a Toa digital pH meter (type HM-10A) with an accuracy of better than  $\pm 0.05$ . The sample solutions for differential scanning calorimetry (DSC) were prepared by sonication with a total concentration of 20–40 mM at pH 3. The solution was sealed in a Ag sample pan and DSC thermograms were obtained with a heating rate of 2 °C/min with a Daini-Seikosha SSC-560 instrument. The detail of the DSC measurement is given elsewhere.<sup>13</sup> The electron micrograph of the aqueous aggregate was obtained with a Hitachi H-500 instrument, as described before.<sup>14</sup> The molecular weight of aqueous aggregates was determined by a Toyo Soda LS-8 light scattering apparatus.<sup>15</sup>

### Results

**Aggregation Behavior.** Azobenzene amphiphile **1** forms globular aggregates, as indicated by electron microscopy.<sup>15,16</sup> The DSC and electron microscopic evidence suggests that the aggregate is a collection of fragmentary bilayer lamellae. Azophenyl ester **2** is expected to give similar bilayer aggregates. An electron micrograph of an aqueous dispersion of **2** stained by uranyl acetate, shows that lamellar aggregates are present abundantly. The layer width is 70–90 Å and is approximately twice the molecular length of **2** (45 Å as estimated from the CPK molecular model). The observed layer width and the presence of the crystal-to-liquid

(9) This salt was prepared by refluxing an ethanol solution of L-histidine and 2.5 equiv of *p*-toluenesulfonic acid: yield 70%; mp 118–120 °C (lit.<sup>10</sup> 120 °C).

(10) Kato, T.; Makizumi, K.; Ohno, M.; Izumiya, N. *Nippon Kagaku Zasshi* **1962**, *83*, 1151–1154.

(11) Bodanszky, M.; du Vigneaud, B. *J. Am. Chem. Soc.* **1959**, *81*, 5688–5691.

(12) Okahata, Y.; Ando, R.; Kunitake, T. *Bull. Chem. Soc. Jpn.* **1979**, *52*, 3647–3653.

(13) Okahata, Y.; Ando, R.; Kunitake, T. *Ber. Bunsenges. Phys. Chem.* **1981**, *85*, 789–798.

(14) Kunitake, T.; Okahata, Y. *J. Am. Chem. Soc.* **1980**, *102*, 549–553.

(15) Kunitake, T.; Okahata, Y.; Shimomura, M.; Yasunaka, S.; Takarabe, K. *J. Am. Chem. Soc.* **1981**, *103*, 5401–5413.

(16) Kunitake, T.; Nakashima, N.; Shimomura, M.; Okahata, Y.; Kano, K.; Ogawa, T. *J. Am. Chem. Soc.* **1980**, *102*, 6642–6644.

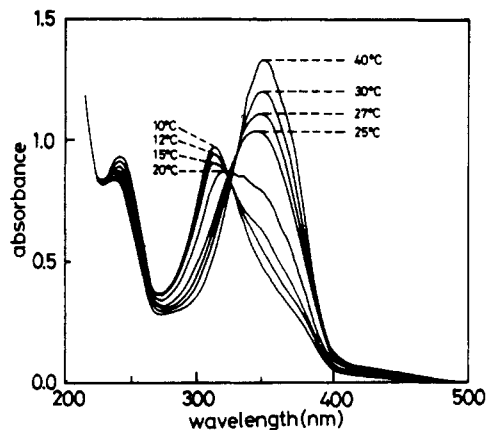


**Figure 1.** Temperature dependence of the absorption spectrum of azobenzene substrate **2** in the bilayer matrix of  $2C_{16}N+2C_1$ . pH 5.3, 0.01 M acetate buffer,  $\mu = 0.02$  (KCl);  $[2] = 5.0 \times 10^{-5}$  M,  $[2C_{16}N+2C_1] = 5.0 \times 10^{-4}$  M.

crystal phase transition clearly indicate formation of the bilayer structure. The bilayer structure of **2** is developed better than that of **1**. This difference must be produced by the presence of the ester unit in **2** that promotes the intermolecular interaction. The importance of the dipolar group as a structural element to promote the molecular assemblage has been discussed in a previous paper from these laboratories.<sup>15</sup>

Electron microscopy could not be applied to the catalyst amphiphile, because it formed precipitates upon addition of staining agents (uranyl acetate, etc.). Therefore, the bilayer formation was inferred from the following data. (1) The molecular weight of an aqueous dispersion was  $1.0 \times 10^8$ , as determined by the light scattering method. The conventional micelle possesses molecular weight of  $10^4$ – $10^5$ , and the molecular weight of the bilayer vesicle is usually  $10^6$ – $10^7$ .<sup>15</sup> Therefore, the observed molecular weight suggests formation of very large (probably lamellar) aggregates. (2) An endothermic peak ( $\Delta H = 3.0$  kcal/mol) was found at 54.5 °C in the DSC study. This is derived from the crystal-to-liquid crystal phase transition of the bilayer. (3)  $\lambda_{\max}$  of  $C_{12}AzoC_{11}His$  is situated at 317 nm in water at 30 °C. The observed blue shift (from 358 nm in ethanol) is attributable to extensive stacking of the azobenzene chromophore and is characteristic of bilayer-forming azobenzene derivatives.<sup>7</sup> The peak shifts to 337 nm at temperatures above 55 °C, indicating lessened chromophore stacking due to phase transition from the crystalline to liquid-crystalline bilayer.

**Spectroscopic Detection of the Substrate Cluster.** The absorption maximum of amphiphile **2** is located at 348–350 nm in methanol, ethanol, and  $CHCl_3$  and at 342 nm in benzene. In water, it undergoes blue shifts due to chromophore stacking: 323 nm at 10 °C and 337 nm at 55 °C. The temperature dependence

**Table I.** Absorption Maxima of Azobenzene Substrate **2** in Various Matrices<sup>a</sup>

matrix	$\lambda_{\max}$ , nm	
	10 °C	40 °C
none	323	337 <sup>b</sup>
$2C_{12}N+2C_1$	348	348
$2C_{14}N+2C_1$	315	349
$2C_{16}N+2C_1$	311	350
$2C_{18}N+2C_1$	310	350
$C_{18}C_8N+2C_1$	348	348
Triton X-100	348	348
POOA	348	348

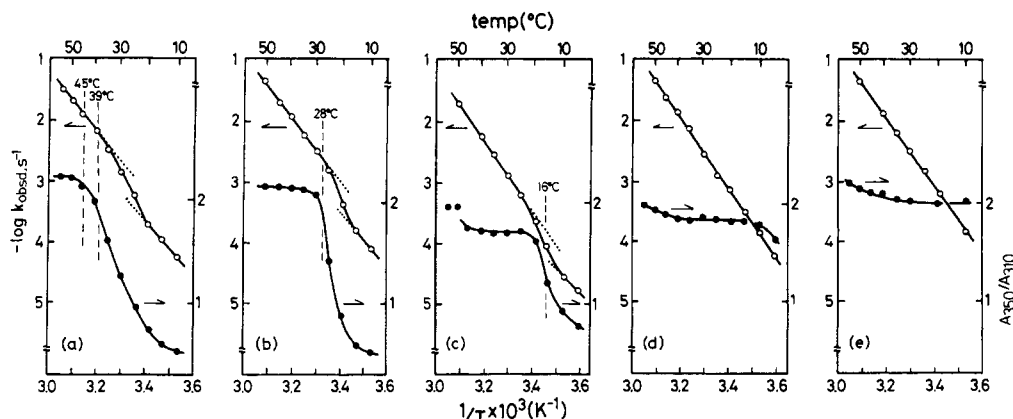
<sup>a</sup> pH 5.3, 0.01 M acetate buffer,  $\mu = 0.02$  (KCl);  $[matrix] = 5 \times 10^{-4}$  M,  $[2] = 5 \times 10^{-5}$  M. <sup>b</sup> 55 °C.

of the blue shift indicates that the orientation of the azobenzene chromophore is affected by the fluidity change of the bilayer.

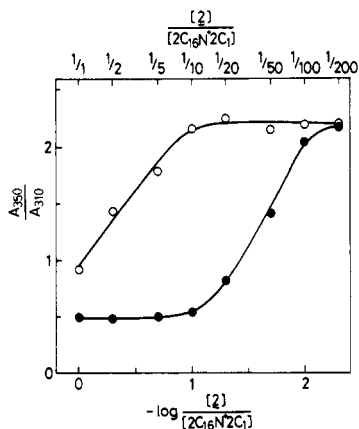
Subsequently, absorption spectra were measured in the presence of various aggregates (molar ratio, 1:10). A typical spectral change with temperature is shown in Figure 1 in the case of the  $2C_{16}N+2C_1$  bilayer matrix. The absorption maximum is situated at 311 nm in the low-temperature range (10–15 °C) and 350 nm in the high-temperature range (25–40 °C). The spectral change is drastic at 15–25 °C. This spectral behavior is quite similar to that of **1** that was reported before.<sup>7</sup> The  $\lambda_{\max}$  value in the high-temperature region is the same as that observed in common organic solvents (see above), and therefore, the blue shift in the low-temperature region is attributed to stacking of the azobenzene chromophore caused by phase separation. In this case, however, a unique isosbestic point was not observed. Thus, the conversion between the isolated and clustered species of the substrate cannot be a simple, two-state process. This problem will be discussed later in this paper.

Table I summarizes  $\lambda_{\max}$  of the substrate in various aggregate matrices at 10 and 40 °C. In all cases at 40 °C,  $\lambda_{\max}$  is located at 348–350 nm in the presence of the matrix, showing the presence of the isolated chromophore. The blue shift was observed upon cooling to 10 °C in the bilayer matrices of  $2C_{14}N+2C_1$ ,  $2C_{16}N+2C_1$ , and  $2C_{18}N+2C_1$ . The micellar aggregates ( $C_{18}C_8N+2C_1$ , Triton X-100, and POOA) do not induce the blue shift. The blue shift was also not observed for the  $2C_{12}N+2C_1$  bilayer matrix, which is in the liquid-crystalline state even at 10 °C.

The absorbance ratio  $A_{350}/A_{310}$  can be used as a semiquantitative measure of disintegration of the azobenzene cluster. As shown in Figure 2, the ratio changes with temperature for the bilayer matrix of  $2C_{14}N+2C_1$ ,  $2C_{16}N+2C_1$ , and  $2C_{18}N+2C_1$ . These changes occur in the same temperature ranges as those of DSC peaks of the respective matrix membrane. No temperature dependence is observed for the  $2C_{12}N+2C_1$  membrane whose phase transition does not exist in the given temperature range. Thus,



**Figure 2.** Temperature dependence of phase separation of substrate **2** and the Arrhenius plots of its alkaline hydrolysis. pH 8.6–8.7, 0.02 M borate buffer,  $\mu = 0.01$  (KCl);  $[substrate] = 7.0 \times 10^{-5}$  M,  $[matrix] = 7.0 \times 10^{-4}$  M. Matrix: (a)  $2C_{18}N+2C_1$ ; (b)  $2C_{16}N+2C_1$ ; (c)  $2C_{14}N+2C_1$ ; (d)  $2C_{12}N+2C_1$ ; (e)  $C_{18}C_8N+2C_1$ .



**Figure 3.** Influence of the molar ratio on dissociation of the cluster in the  $2C_{16}N+2C_1$  matrix. pH 5.3, 0.01 M acetate buffer,  $\mu = 0.02$  (KCl);  $[2C_{16}N+2C_1] = 5.0 \times 10^{-4}$  M. (O) 40 °C; (●) 10 °C.

it is strongly suggested that the formation of the azobenzene cluster is induced by crystallization (liquid crystal-to-crystal phase transition) of the matrix membrane. The cluster formation is not detected in the fluid (liquid crystalline) membrane matrix under the conditions used.

However, this conclusion holds true only under a fixed molar ratio (1:10) of the two amphiphiles (2 and 3). Figure 3 illustrates the dependence of  $A_{350}/A_{310}$  on the molar ratio of 2 and  $2C_{16}N+2C_1$  in the mixed membrane. The concentration of  $2C_{16}N+2C_1$  was fixed at  $5.0 \times 10^{-4}$  M and that of 2 was varied between  $5.0 \times 10^{-4}$  and  $2.5 \times 10^{-6}$  M. The molar ratio changes from 1:1 to 1:200. Two temperatures (10 and 40 °C) are selected in this experiment, because they are below and above the phase transition of the matrix membrane ( $T_c$ (peak top) = 28 °C). At 10 °C where the matrix membrane is in the crystalline phase, the azobenzene chromophore is present as clusters if the molar ratio is 1:1–1:10. As the molar ratio decreases below 1:10, the isolated chromophore increases and the cluster seemingly disappears at 1:200. This equilibrium between the isolated and clustered chromophore moves toward the isolated species at 40 °C where the matrix membrane is in the liquid-crystalline state. At this temperature, the two species coexist at molar ratios of 1:1–1:10, but only the isolated species are present at molar ratios of 1:10–1:200. These data indicate that the substrate cluster can be produced in the crystalline as well as liquid-crystalline membrane matrices by using appropriate concentrations (in the matrix).

**Detection of Substrate Cluster by Differential Scanning Calorimetry (DSC).** Formation of the substrate cluster can be readily detected by DSC. Figure 4 shows DSC charts of aqueous dispersions of the mixed membrane of substrate amphiphile 2 and  $2C_{16}N+2C_1$ . The phase-transition temperature ( $T_c$ ) and the transition enthalpy ( $\Delta H$ ) of the  $2C_{16}N+2C_1$  membrane (sonicated sample) are 28.0 °C (peak-top temperature) and 5.7 kcal/mol, respectively.  $T_c$  and  $\Delta H$  of the substrate bilayer are 50.0 °C and 4.5 kcal/mol, respectively. A 1:1 mixture of the membrane components gives two endothermic peaks at 28.5 and 51.5 °C that correspond to  $T_c$  of  $2C_{16}N+2C_1$  and 2, respectively. This establishes beyond doubt the presence of separate clusters. It is interesting that  $\Delta H$  for 2 (5.4 kcal/mol) in the mixed membrane is greater than that in the single-component membrane (4.5 kcal/mol). In contrast,  $\Delta H$  of  $2C_{16}N+2C_1$  is smaller in the phase-separated membrane (3.0 kcal/mol) than in the single-component membrane (5.7 kcal/mol). These  $\Delta H$  data suggest that the molecular orientation of the azobenzene amphiphile is improved in the mixed membrane from in the single-component membrane. The 50 °C peak becomes broader and  $\Delta H$  becomes smaller as the molar ratio of 2 decreases (1:1–1:10) (Figure 4b–f). This trend again agrees with the decrease in the substrate cluster observed spectroscopically (the ascending portion of the 40 °C curve of Figure 3).

The major peak for  $2C_{16}N+2C_1$  is located at the identical temperature (28.5 °C), in spite of the presence of 2. However,

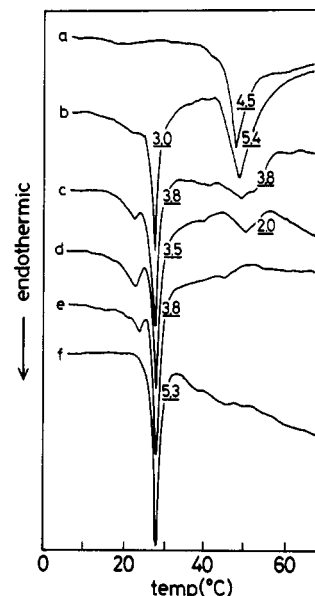


**Figure 4.** DSC thermograms of mixed membranes of 2 and  $2C_{16}N+2C_1$  in water. Concentrations of 2 and  $2C_{16}N+2C_1$  are respectively; (a) 20 and 0 mM; (b) 20 and 20 mM; (c) 15 and 20 mM; (d) 10 and 20 mM; (e) 5 and 20 mM; (f) 2 and 20 mM. The number denotes  $\Delta H$  (kcal/mol) of the respective peaks.

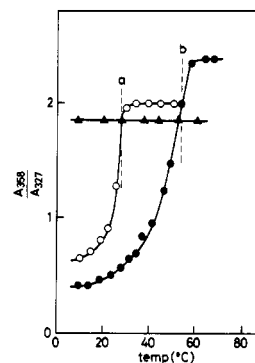


**Figure 5.** Temperature dependence of absorbance ratio,  $A_{358}/A_{327}$ , for catalyst amphiphiles in dialkylammonium matrices. pH 7.7 unless indicated otherwise, 0.02 M borate buffer,  $\mu = 0.02$  (KCl); [catalyst] =  $5.0 \times 10^{-3}$  M, [matrix] =  $5.0 \times 10^{-4}$  M. Temperatures a and b are  $T_c$  of aqueous  $2C_{16}N+2C_1$  and  $C_{12}AzoC_{11}His$  (pH 4.3), respectively. (O)  $C_{12}AzoC_{11}His/2C_{16}N+2C_1$ ; (●)  $C_{12}AzoC_{11}His/2C_{16}N+2C_1$ , pH 4.3; (▲)  $C_{12}AzoC_{11}His/C_{18}C_8N+2C_1$ .

$\Delta H$  of this peak becomes smaller with increasing amounts of 2, and a minor peak appears at 23–25 °C. This implies the formation of less aligned areas of the  $2C_{16}N+2C_1$  bilayer at the interface of the domain of the substrate cluster.

**Formation of Catalyst Cluster.** The absorption spectrum of the catalyst amphiphile  $C_{12}AzoC_{11}His$ , imbedded in 10 times excess of aqueous  $2C_{16}N+2C_1$  (pH 7.7), possesses  $\lambda_{max}$  at 327 and 357 nm at low- and high-temperature regions, respectively. The spectral change (blue shift at low temperatures) is induced by phase separation of the azobenzene amphiphile, as mentioned above. The phase separation cannot be expressed by a simple two-state equilibrium in this case as well, since a single isosbestic point is not observed.

The temperature dependence is shown in Figure 5 (open circle) by plotting the absorbance ratio of the monomeric and cluster species against temperature. The absorbance ratio changes drastically at 20–30 °C in coincidence with the phase-transition temperature (28 °C) of the matrix membrane. When  $C_{18}C_8N+2C_1$ , which does not produce the bilayer assembly,<sup>17</sup> is

(17) Kunitake, T.; Okahata, Y.; Tamaki, K.; Kumamaru, F.; Takayanagi, M. *Chem. Lett.* 1977, 387–390.

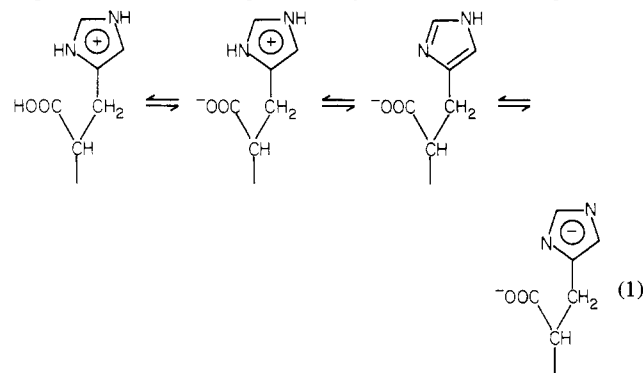
**Table II.** Absorption Maxima of  $C_{12}AzoC_{11}His$  Catalyst in the  $2C_{16}N^+2C_1$  Matrix<sup>a</sup>

medium pH	histidine head group	$\lambda_{max}$ , nm	
		10 °C	40 °C
11.5 (0.01 N NaOH)	anionic	333	358
8.0 (0.02 M borate)	anionic	327	358
4.3 (0.02 M acetate)	zwitterionic	317	357, 317 <sup>b</sup>
2.4 (0.01 N HCl)	cationic	314	355, 317 <sup>b</sup>

<sup>a</sup>  $[2C_{16}N^+2C_1] = 7.0 \times 10^{-4}$  M,  $[C_{12}AzoC_{11}His] = 7.0 \times 10^{-5}$  M. <sup>b</sup> Minor peak.

used as the matrix in place of  $2C_{16}N^+2C_1$ , the monomer spectrum is observed in the whole temperature range (filled triangle). These spectral data indicate that the membrane catalyst,  $C_{12}AzoC_{11}His$ , forms clusters in the rigid (below  $T_c$ ) membrane matrix of  $2C_{16}N^+2C_1$  but exists as the isolated species in the fluid (above  $T_c$ ) membrane matrix and in the nonmembranous matrix of  $C_{18}C_8N^+2C_1$ .

**Effect of Medium pH and Concentration on Formation of Catalyst Cluster.** The histidine head group can be cationic, zwitterionic, anionic, or dianionic, depending on the medium pH (eq 1). The isoelectric point of acylated histidine is reported to



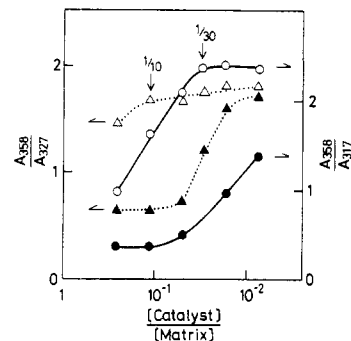
be pH 4.0,<sup>18</sup> and the imidazolyl anion is usually produced at pH much above 9.<sup>19</sup>

Figure 5 also shows the monomer–cluster equilibrium observed at pH 4.3 instead of pH 7.7. The change in the absorbance ratio occurs at higher temperatures (40–55 °C). This temperature range corresponds to that of phase transition of  $C_{12}AzoC_{11}His$  ( $T_c = 54.5$  °C) rather than that of the matrix membrane. The histidine head group is predominantly zwitterionic at pH 4.3 and anionic at pH 7.7. Thus the membrane catalyst can exist as clusters even in the fluid bilayer matrix, if the head group is zwitterionic. Table II summarizes  $\lambda_{max}$  of the catalyst in the  $2C_{16}N^+2C_1$  matrix at different pH's and temperatures. The spectrum consists of the monomer species ( $\lambda_{max}$  358 nm) at pH >8 and 40 °C. The cluster peak appears as minor peaks at 317 nm under acidic condition at the same temperature. When the matrix is in the crystalline phase (10 °C), the monomer peak disappears almost completely. It is interesting, however, that  $\lambda_{max}$  of the cluster species changes from 333 to 314 nm with lowering pH's. The chromophore interaction is apparently influenced by the charged state of the histidine head group. The extent of the blue shift is shown to reflect the cluster structure,<sup>20</sup> and the catalyst amphiphile with the anionic head (at pH >8) appears to form loosely stacked (and/or small) clusters ( $\lambda_{max}$  333–327 nm) in the cationic bilayer matrix. The zwitterionic and cationic histidine heads, which are predominant at pH 4.3 and 2.4, respectively, result in the better stacked clusters (larger blue shifts). This  $\lambda_{max}$  variation lies in the same range as that observed in the course of phase transition of the single-component membrane of the same amphiphile (337–317 nm).

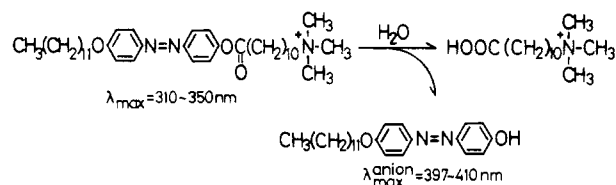
(18) Gitler, C. G.; Ochoa-Solano, A. *J. Am. Chem. Soc.* **1968**, *90*, 5004–5009.

(19) Bruice, T. C.; Benkovic, S. J. "Bioorganic Mechanisms"; W. A. Benjamin: New York, 1966; Vol. I, Chapter 1.

(20) Shimomura, M., unpublished results in these laboratories.



**Figure 6.** Influence of the component molar ratio on the absorbance ratio (monomer/cluster).  $[C_{12}AzoC_{11}His] = 5.0 \times 10^{-5}$  M,  $[2C_{16}N^+2C_1] = 5.0 \times 10^{-4}$  M; pH 4.3, 0.01 M acetate buffer,  $\mu = 0.01$  (KCl). (O) 40 °C; (●) 10 °C. pH 8.0, 0.02 M borate buffer,  $\mu = 0.01$  (KCl). (Δ) 40 °C; (▲) 10 °C.

**Scheme 1**

The monomer–cluster equilibrium as affected by the concentration of the catalyst molecules in the matrix is shown in Figure 6. At 40 °C, the anionic (pH 8) catalyst amphiphile is completely dispersed as monomer at molar ratios of 1:10 or less, while the zwitterionic catalyst (pH 4.3) becomes molecularly dispersed only at 1:30 or less. The cluster formation is promoted in the rigid matrix at 10 °C, and the zwitterionic catalyst remains partially as clusters even at a molar ratio of 1:100.

**Phase Separation of Catalyst Induced by  $Cu^{2+}$  Addition.** Phase separation in biomembranes and liposomes is induced by addition of inorganic ions.<sup>21,22</sup> When  $Ca^{2+}$  is used as added ion, its interaction with phosphatidylserine and phosphatidylethanolamine gives rise to phase separation. Similar situations may arise for the histidine-containing amphiphile with  $Cu^{2+}$  ion. As shown in Figure 6, the catalyst amphiphile is molecularly dispersed in the  $2C_{16}N^+2C_1$  matrix (10 times excess) at 40 °C and pH 8.0. Upon addition of  $Cu^{2+}$  ion, the monomer peak at 358 nm decreases and the cluster peak at 317 nm increases with an isosbestic point at 330 nm. The spectral change suggests formation of the 1:2 ( $Cu^{2+}/His$ ) complex at 40 °C. The absorption spectrum at this point (monomer + cluster) is identical with that of the zwitterionic species (at pH 4.3) without addition of  $Cu^{2+}$  ion. Therefore, neutralization of the surface charge is mainly responsible for the spectral change.

The cluster species are already present at 10 °C prior to  $Cu^{2+}$  addition. The addition of  $Cu^{2+}$  produces a blue shift of ca. 10 nm and a further decrease in the monomer peak, and the spectrum becomes very similar to that of the zwitterionic species. Interestingly, the decrease in the relative absorbance saturates at  $Cu^{2+}/His = 1/4$ .

**Spontaneous Hydrolysis of Substrate Amphiphile.** The spontaneous hydrolysis of substrate **2** in the dialkylammonium bilayer matrix was followed by UV–visible spectroscopy. Figure 7a illustrates typical time courses of the spectral change due to hydrolysis. Substrate **2** gives a single  $\lambda_{max}$  at 350 nm, when it exists as the isolated species in the 10-times excess  $2C_{16}N^+2C_1$  matrix at 40 °C (Table I). The substrate peak diminishes with time, and a new peak of the product phenolate appears at 410 nm. The isosbestic points are at 377, 295, and 254 nm, and the absorbance increase at 410 nm obeys the pseudo-first-order rate law up to

(21) Ohnishi, S., *Adv. Biophys.* **1975**, *8*, 35–82.

(22) Mayer, L. D.; Nelsestuen, G. L., *Biochemistry* **1981**, *20*, 2457–2463.

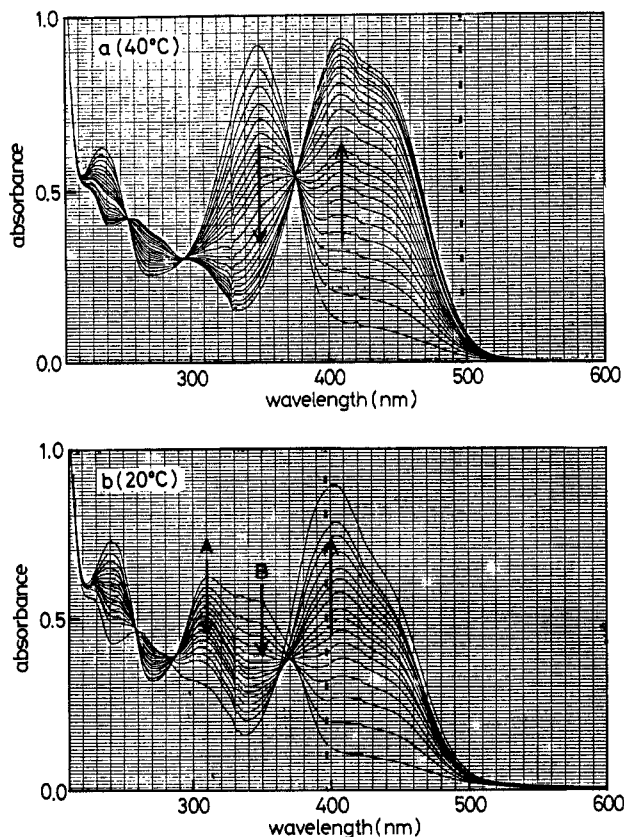


**Figure 7.** Spectral change due to hydrolysis of substrate 2 in the matrix of  $2C_{16}N^+2C_1$ .  $[2] = 7.0 \times 10^{-5}$  M,  $[2C_{16}N^+2C_1] = 7.0 \times 10^{-4}$  M. (a) 40 °C, pH 9.6, 0.02 M borate buffer,  $\mu = 0.01$  (KCl); (b) 20 °C, pH 11.7, 0.01 N NaOH,  $\mu = 0.01$  (KCl).

90% conversion. Thus, it is concluded that the alkaline hydrolysis (eq 2) proceeds without kinetic complications in the membrane matrix at 40 °C (Scheme I).

A different situation arises at 20 °C where the matrix membrane is in the crystalline phase. As shown in Figure 7b, the substrate gives  $\lambda_{max}$  at 310 nm (A) and 350 nm (B) due to the coexistence of the isolated (monomer) and cluster species. Both peaks (A and B) disappear with time and the product peak appears at 400 nm correspondingly. However, peak B disappears faster than peak A, and an isosbestic point does not exist near 380 nm.

Sufficiently linear pseudo-first-order plots are found at 10 and 40 °C under these particular conditions. The substrate molecule is present predominantly as clusters at 10 °C and as monomers at 40 °C. A pH-rate profile (pH- $\log k$ ) at 10 °C gives a linear relation with slope of unity in the range of pH 9–12. Therefore, it is concluded that the reaction proceeds via the conventional kinetics of alkaline hydrolysis even for the cluster species. In contrast, the reaction does not obey the pseudo-first-order kinetics at 20 °C. The monomer and cluster species coexist at this temperature, as can be seen from Figure 7b. The matrix membrane should also be composed of the crystalline and liquid-crystalline phases at 20 °C. Apparently, equilibration of the two substrate species is slower than the reaction, and the pseudo-first-order kinetics do not hold at this temperature.

The influence of the phase separation on the reaction rate is also reflected in the Arrhenius plots, as included in Figure 2. The rate constant,  $k_{obsd}$ , was usually obtained from the pseudo-first-order plots up to 50% conversion. However, when the reaction is slow especially at low temperatures (below  $T_c$  of the matrix membrane), the initial rate (up to 30% conversion) was used. This procedure may introduce some degrees of error, because the product formation is biphasic as shown in Figure 7, and the initial rate represents the reaction of the monomeric substrate rather than that of the cluster species. The apparent rate at a later stage of reaction would be a better index of the reactivity of the substrate cluster.

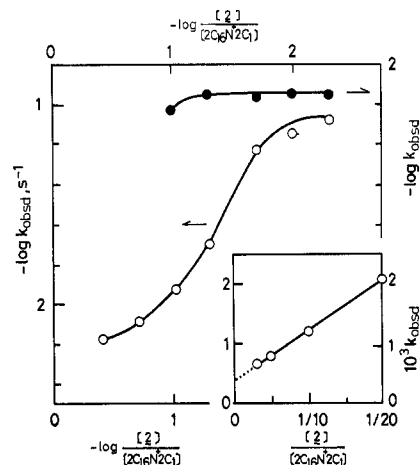


**Figure 8.** Effect of the substrate concentration on the hydrolysis rate in the bilayer matrix of  $2C_{16}N^+2C_1$ ,  $[2C_{16}N^+2C_1] = 1.0 \times 10^{-3}$  M. (●) 40 °C, pH 9.8; (○) 10 °C, pH 11.8.

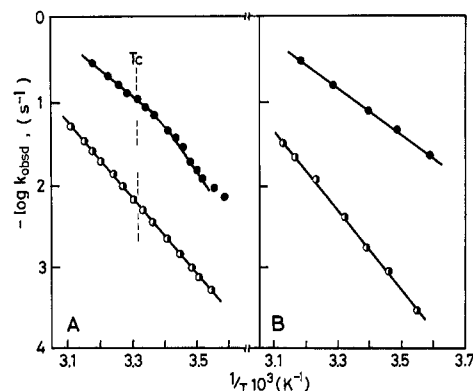


**Figure 9.** Arrhenius plots of hydrolysis. The broken line indicates  $T_c$  of the  $2C_{16}N^+2C_1$  matrix. pH 7.6 to 7.7, 0.02 M borate buffer,  $\mu = 0.01$  (KCl); [catalyst] =  $7.0 \times 10^{-5}$  M, [Z-Phe-PNP] =  $2.0 \times 10^{-5}$  M, [matrix] =  $7.0 \times 10^{-4}$  M. A, ( $2C_{16}N^+2C_1$  matrix): (●)  $C_{12}AzoC_{11}His$  catalyst; (○) no catalyst. B, ( $C_{18}C_8N^+2C_1$  matrix): (●)  $C_{12}AzoC_{11}His$  catalyst; (○) no catalyst.

The Arrhenius plots in the bilayer matrix of  $2C_{18}N^+2C_1$ ,  $2C_{16}N^+2C_1$ , and  $2C_{14}N^+2C_1$  are composed of two lines. The inflection regions coincide with the temperature range where phase separation of the substrate occurs. The Arrhenius plots in the  $2C_{12}N^+2C_1$  and  $C_{18}C_8N^+2C_1$  matrices are represented by single straight lines. The  $A_{350}/A_{310}$  value is essentially constant in these matrices. Thus, it is established that the inflections are induced by phase separation, which causes the change of the distribution of the substrate molecule in the bilayer matrix and the resulting reactivity change.

The formation of the substrate cluster is also affected by the molar ratio of the substrate and the matrix, as shown in Figure 3. Therefore, the dependence of the apparent rate on the substrate concentration was examined in the case of the  $2C_{16}N^+2C_1$  bilayer. The results are shown in Figure 8. The apparent rate constant is virtually the same at 40 °C for the molar ratios ranging from 1:10 to 1:200. This concentration independence is similar to that observed for  $A_{350}/A_{310}$  (Figure 3). At 10 °C, however, the rate constant shows a gradual decrease with the increase in the molar ratio. The rate constant at a molar ratio of 1:200 ( $k_{obsd} = 0.0787$  s $^{-1}$ ) is 10 times larger than that obtained at a molar ratio of 1:10 ( $k_{obsd} = 0.0078$  s $^{-1}$ ). The molar ratio dependence of the rate at 10 °C is similar to the dependency of  $A_{350}/A_{310}$  of Figure 3 at the same temperature, except in the high molar ratio region.  $A_{350}/A_{310}$  reaches a constant value at a molar ratio above 1:10 in Figure 3, whereas  $k_{obsd}$  keeps descending in the same region. This discrepancy is interpreted as follows: 10 mol % (relative to the matrix amphiphile) of the substrate amphiphile is present as the monomer species in this region. These monomer species cannot

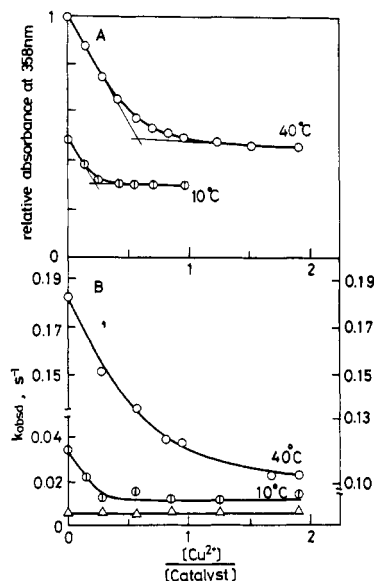


**Figure 10.** (A) Effect of  $\text{Cu}^{2+}$  addition on the relative absorbance at 358 nm and (B) the catalytic efficiency of  $\text{C}_{12}\text{AzoC}_{11}\text{His}$  in the  $2\text{C}_{16}\text{N}^+2\text{C}_1$  matrix. pH 7.7, 0.02 M borate buffer,  $\mu = 0.01$  (KCl); [catalyst] =  $7.1 \times 10^{-5}$  M, [matrix] =  $7.1 \times 10^{-4}$  M, [Z-Phe-PNP (substrate)] =  $2.0 \times 10^{-5}$  M. (O) 40 °C; (◊) 10 °C; (Δ) spontaneous hydrolysis at 40 °C.

be detected spectroscopically because large excesses of the cluster species are present. However, the overall reactivity is still affected by the decrease in the monomer species, because the monomer species are more reactive than the cluster species. The influence of the monomer species can be eliminated in the plots of  $k_{\text{obsd}}$  against  $[\text{substrate}]/[2\text{C}_{16}\text{N}^+2\text{C}_1]$  inserted in Figure 8. The intercept,  $0.0043 \text{ s}^{-1}$ , gives the reactivity of the substrate cluster alone. This value is  $1/19$  of  $k_{\text{obsd}}$  of the monomer species.

**Hydrolysis of Phenyl Ester Catalyzed by Bilayer-Forming Amphiphile.** The catalyzed hydrolysis of Z-Phe-PNP substrate (4) in the  $2\text{C}_{16}\text{N}^+2\text{C}_1$  bilayer matrix is very fast:  $k_{2,\text{obsd}}$  (apparent second-order rate constant) = ca.  $3000 \text{ M}^{-1} \text{ s}^{-1}$ . This large value is close to that of the same substrate catalyzed by a long-chain acylhistidine.<sup>23</sup> The Arrhenius plots of the uncatalyzed hydrolysis shown in Figure 9A give a linear relation. On the other hand, the hydrolysis catalyzed by  $\text{C}_{12}\text{AzoC}_{11}\text{His}$  produces the Arrhenius plots seemingly composed of three linear portions. The major inflection point (ca. 25 °C) is close to  $T_c$  of the matrix membrane. The catalyst cluster is formed extensively at temperatures below  $T_c$  (Figure 5), and therefore, the steeper slope observed in the low-temperature region implies that the clustered catalyst is less reactive than the monomeric counterpart.

When the micellar matrix of  $\text{C}_{18}\text{C}_8\text{N}^+2\text{C}_1$  is used, simple Arrhenius plots are observed even for the membrane-forming catalyst (Figure 9B). This result is consistent with the presence of the molecularly dispersed catalyst in the micellar matrix.

**Effect of  $\text{Cu}^{2+}$  on Catalytic Hydrolysis.** As discussed above, the cluster formation of  $\text{C}_{12}\text{AzoC}_{11}\text{His}$  is promoted by  $\text{Cu}^{2+}$  addition. Therefore, it is expected that the catalytic behavior is affected by the  $\text{Cu}^{2+}$  ion. Figure 10B describes rate changes by  $\text{Cu}^{2+}$  addition. The uncatalyzed reaction is not influenced by  $\text{Cu}^{2+}$ . The rate of the catalytic hydrolysis by  $\text{C}_{12}\text{AzoC}_{11}\text{His}$  decreases with  $\text{Cu}^{2+}$  addition in a manner similar to that of the cluster formation shown in Figure 10A. The rate decrease, therefore, may be attributed to the cluster formation, since the cluster species is less reactive than the monomer species. Similar results are obtained at 10 °C.

## Discussion

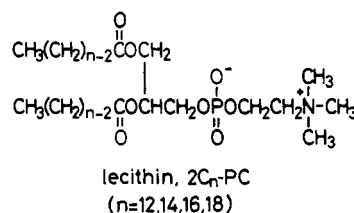
**Phase Separation of Substrate Amphiphile.** The ease of phase separation of substrate amphiphile 2 is affected by (1) the con-

centration (molar ratio) of the amphiphile in the bilayer matrix and (2) the physical state (crystalline or liquid crystalline) of the matrix membrane. The influence of the physical state of the substrate amphiphile could not be examined in the present study, since its  $T_c$  (50 °C) is at the higher end of the temperature range used.

The isolated and clustered species of the substrate amphiphile should coexist under practically all the experimental conditions. For instance,  $A_{350}/A_{310}$  at 40 °C (Figure 3) is constant in the range of  $[\text{substrate}]/[2\text{C}_{16}\text{N}^+2\text{C}_1]$  of 1:200–1:10. The  $A_{350}/A_{310}$  value starts to decrease, when the molar ratio increases beyond 1:10. This result indicates that 10 mol % of the substrate amphiphile is miscible with the liquid-crystalline  $2\text{C}_{16}\text{N}^+2\text{C}_1$  matrix. When the concentration is greater than 10 mol %, the extra substrate molecule forms a separate phase. The miscibility diminishes drastically if the matrix membrane is in the crystalline phase. At 10 °C where the matrix membrane is rigid, the  $A_{350}/A_{310}$  value reaches the saturation value only at the molar ratio of 1:200 or lower. This means that the substrate amphiphile is miscible with the rigid  $2\text{C}_{16}\text{N}^+2\text{C}_1$  matrix by the amount of 0.5% or less.

The DSC data support these interpretations. In Figure 4, the 28.5 °C peak possesses analogous shapes in spite of the presence of different amounts of the substrate amphiphile. This means that the matrix phase is essentially not perturbed at the onset of the phase transition.

A detailed analysis of phase separation (component miscibility) in the phospholipid bilayer was performed by Mabrey and Sturtevant.<sup>24</sup>



They examined the DSC behavior of mixed membranes of lecithins with different acyl chain lengths. Mixtures of  $2\text{C}_{12}\text{-PC}$  and  $2\text{C}_{18}\text{-PC}$  gave separate DSC peaks, which indicate phase separation. The  $T_c$  value for  $2\text{C}_{12}\text{-PC}$  was almost invariable at various mixing ratios but that for  $2\text{C}_{18}\text{-PC}$  was lowered with increasing contents of  $2\text{C}_{12}\text{-PC}$ . They concluded from these data that  $2\text{C}_{18}\text{-PC}$  is almost immiscible in the domain of  $2\text{C}_{12}\text{-PC}$  but that  $2\text{C}_{12}\text{-PC}$  is soluble by  $15 \pm 5$  mol % in the domain of  $2\text{C}_{18}\text{-PC}$ . This different miscibility behavior may be anticipated, since the DSC experiment (in the heating scan) describes the miscibility of  $2\text{C}_{12}\text{-PC}$  only in the crystalline  $2\text{C}_{18}\text{-PC}$  domain and the miscibility of  $2\text{C}_{18}\text{-PC}$  only in the liquid-crystalline  $2\text{C}_{12}\text{-PC}$  domain. The miscibility of a given lecithin would naturally depend on the physical state of the matrix membrane: better miscibility in the liquid-crystalline matrix. The mutual solubility is improved when the difference in the acyl chain length is small; the complete miscibility was observed for the combinations of  $2\text{C}_{18}\text{-PC}$  and  $2\text{C}_{16}\text{-PC}$ , and  $2\text{C}_{16}\text{-PC}$  and  $2\text{C}_{14}\text{-PC}$  with eutectic points related to the mixing ratio.

It was noted in these laboratories that dialkylammonium salts with different alkyl chain length show generally good miscibility.<sup>25</sup> The miscibility depends on the structural similarity, and single-chain amphiphiles such as 1 and 2 may not be highly miscible with dialkyl amphiphiles.

The nature of phase separation can be inferred also from the change in the transition enthalpy ( $\Delta H$ ). The  $\Delta H$  value for the single-component membrane of  $2\text{C}_{16}\text{N}^+2\text{C}_1$  is 5.7 kcal/mol. This value decreases to 5.3–3.0 kcal/mol by addition of 2 (molar ratio 1:10–1:1, respectively). If the 28.5 °C peak of the mixed membrane is derived from the domain of pure  $2\text{C}_{16}\text{N}^+2\text{C}_1$  (because of the similarity of the peak position and shape to those of pure

(23) Yamada, K.; Shosenji, H.; Ihara, H.; Otsubo, Y. *Tetrahedron Lett.* 1979, 2529–2532.

(24) Mabrey, S.; Sturtevant, J. M. *Proc. Natl. Acad. Sci.* 1976, 73, 3862–3866.

(25) Unpublished results in these laboratories.

$2C_{16}N^+2C_1$  membrane), the  $\Delta H$  decrease may be attributed to the formation of the eutectic domain of the substrate and  $2C_{16}N^+2C_1$ . The latter domain either does not contribute to  $\Delta H$  or appears as a peak at 25.5 °C ( $\Delta H = 0.5$ – $1$  kcal/mol) in Figure 4.

On the other hand,  $\Delta H$  of the substrate peak at 50 °C is 5.4 kcal/mol for the 1:1 mixed membrane. One-tenth of the substrate molecule is miscible with the  $2C_{16}N^+2C_1$  matrix at 40 °C, and the amount of the dissolved species will be greater than 10 mol % at around 50 °C. Therefore,  $\Delta H$  of the pure cluster species should not be smaller than 6 kcal/mol. This value is at least 30% greater than that of the single-component bilayer of the substrate. Apparently, the substrate bilayer is aligned better in the dialkylammonium matrix than in its absence. This presumption is supported by the spectral data:  $\lambda_{max}$  of the substrate as the single-component aggregate is located at 323 nm at 10 °C (below  $T_c$ ) but that in a mixed membrane with  $2C_{16}N^+2C_1$  is at 311 nm (Table I). Since the blue shift for the azobenzene chromophore increases with chromophore stacking,<sup>25</sup> the observed  $\lambda_{max}$  difference reinforces the above conclusion.

Upon further reduction of the molar ratio of the substrate in the  $2C_{16}N^+2C_1$  matrix,  $\Delta H$  of the substrate peak decreases to 3.8 kcal/mol (molar ratio 20:15) and 2.0 kcal/mol (molar ratio 20:10). This decrease is greater than that that can be corrected by the presence of the solubilized substrate. The corrected  $\Delta H$  values are 4.4 and 2.5 kcal/mol, respectively. If the number, not the size, of the substrate domain decreases with its decreasing molar ratio, the corrected  $\Delta H$  value should be constant. That this is not the case indicates that the amount of the substrate amphiphile that does not contribute to  $\Delta H$  increases with the decrease in the molar ratio. This is explained readily by assuming the decrease in the size, not the number, of the domain, since the membrane component at the interface of domains would not make much contribution to  $\Delta H$  and the interfacial component increases with decreasing domain sizes.

**Phase Separation of Catalyst Amphiphile.** The phase separation of catalyst amphiphile 3 in the  $2C_{16}N^+2C_1$  matrix is affected by the same factors as those for substrate amphiphile 2: i.e., (1) catalyst concentration in the bilayer matrix and (2) physical state of the matrix membrane. Additional factors (medium pH and  $Cu^{2+}$ ) arise because of the histidine head. As shown in Figure 5, phase separation of the membrane catalyst (anionic species) at a fixed concentration (molar ratio 1:10) occurs as the  $2C_{16}N^+2C_1$  matrix is converted from the liquid-crystalline to crystalline phases. However, the phase separation proceeds at a higher temperature ( $T_c$  of the catalyst), not at  $T_c$  of the matrix, if the catalyst is in the zwitterionic form (pH 4.3). The cluster species also persist at temperatures above  $T_c$ , if the catalyst concentration (molar ratio) is higher; i.e., the concentration effect (Figure 6). The catalyst contains the histidine head group, and therefore, the charge of the head group changes with the medium pH and by complexation with  $Cu^{2+}$  ion (Figures 6 and 10). Phase separation of the anionic species is not extensive in the cationic dialkylammonium matrix. Neutralization of the head group either by the pH change or by complexation with  $Cu^{2+}$  promotes phase separation, as expected from simple electrostatic consideration. The spectral coincidence of the azobenzene chromophore in the catalyst- $Cu^{2+}$  complex with that in the zwitterionic catalyst supports this view.

**Reactivity Change due to Phase Separation. 1. Substrate.** The true reactivity of the clustered substrate may be determined by taking the monomer-cluster equilibrium into consideration. However, the data of Figures 1 and 4 imply that the equilibrium is not straightforward. The temperature dependence of the absorption spectrum (Figure 1) gives two isosbestic points, suggesting that the monomeric substrate is transformed into the cluster species via a separate intermediate stage that is formed at ca. 20 °C. The DSC thermogram of the mixtures of Figure 4 similarly suggests the formation of the intermediate species, since a low-temperature peak (~25 °C) that cannot be attributed to either monomeric or cluster species appears in the intermediate molar ratios. Thus there should exist at least two types of the cluster that are different

in their sizes. It must be noted that the size difference produces the change in the chromophore interaction (i.e., mode of molecular aggregation), as implied by the spectral change. In the same vein, the large cluster possesses an aggregation structure different from that of the single-component substrate bilayer, since their spectral characteristics do not coincide.

It may be assumed for the sake of simplicity that the reaction proceeds from three types of the substrate: monomeric substrate and substrate in small and large clusters. The reactivity of the monomeric substrate is readily estimated at small molar ratios of the substrate in the bilayer matrix and that of the large cluster is estimated from the intercept in the plot of the apparent rate constant against the molar ratio ( $[substrate]/[matrix]$ ). However, the reactivity of the intermediate (small) cluster cannot be determined from the available data.

The substrate cluster, if large enough, is in the crystalline phase under most of the experimental conditions, since its  $T_c$  is 50 °C. The hydroxide ion may not penetrate readily into the rigid substrate cluster. If it does and the tetrahedral intermediate is formed by the OH addition, disposition of the leaving group could be suppressed in the rigid bilayer matrix. This possibility can be examined by changing the nature of the substrate cluster. We are currently studying the reactivity of the cluster of substrates with systematic structural changes. By doing so, the reactivity of the substrate cluster in the crystalline and liquid-crystalline phases can be compared.

As another possibility, the slower rate for the cluster may represent the rate-limiting transfer from the cluster to monomer substrate. In this case the true reacting species is the monomer, and the cluster substrate should have a reactivity much smaller than that observed.

**2. Catalyst.** The apparent activation energy,  $E_a$  of the catalytic hydrolysis was estimated from the slopes of Figure 9 to be 14.5 kcal/mol (28–40 °C) and 26.9 kcal/mol (12–24 °C) in  $2C_{16}N^+2C_1$  and 11.4 kcal/mol (whole temperature range) in  $C_{18}C_8N^+2C_1$ . The phase transition (peak top) temperature of the  $2C_{16}N^+2C_1$  bilayer is 28 °C; therefore,  $E_a$  in the rigid matrix is greater than that in the fluid matrix by 12.4 kcal/mol.

Since the catalyst molecule exists predominantly as cluster species in the rigid matrix and as isolated species in the fluid matrix under the experimental conditions used, the large activation energy observed in the rigid matrix may be attributed to two interrelated factors. One of them is the change in the microenvironment of the catalyst group. The histidine head group is in the anionic form under the hydrolysis conditions, and therefore, it is imbedded in the anionic environment of the cluster. It has been shown that the catalytic activity of acylated histidines is enhanced in the cationic micelle and suppressed in the anionic micelle.<sup>26,27</sup> Thus, the histidine head in the cluster would naturally show reduced reactivity than when it is isolated in the cationic matrix. We showed separately that the reactivity of the anionic catalyst bilayer (no matrix used) is less than  $1/20$  of that of the isolated anionic catalyst in the dialkylammonium matrix.<sup>28</sup> The anionic cluster in the cationic matrix would show an intermediate activity of these extremes. The second factor is the rigidity of the catalyst cluster. As mentioned above, the decreased reactivity of the clustered substrate may be explained by slower penetration of hydroxide ion into the rigid cluster. In the same way, the rigid catalyst cluster would be less reactive toward Z-Phe-PNP substrate.

The membrane catalyst in the micellar ( $C_{18}C_8N^+2C_1$ ) matrix gives an  $E_a$  value (11.4 kcal/mol) close to that obtained in the fluid bilayer matrix. It appears that the peculiarity of the membrane system is lost in these cases.

Addition of  $Cu^{2+}$  ion induced lowering of the catalytic reactivity to one-third of the original value (Figure 10). This lowering

(26) Inoue, T.; Nomura, K.; Kimizuka, H. *Bull. Chem. Soc. Jpn.* 1976, 54, 2072–2078.

(27) Yamada, K.; Shosenji, H.; Ihara, H. *Chem. Lett.* 1979, 491–494.

(28)  $k_{1,obsd} = 0.0058$  s<sup>-1</sup> for  $C_{12}AzoC_{11}His$  ( $3.5 \times 10^{-5}$  M) and Z-Phe-PNP ( $1.0 \times 10^{-5}$  M).  $k_{1,obsd} = 0.120$  s<sup>-1</sup> for  $C_{12}AzoC_{11}His$  ( $3.5 \times 10^{-5}$  M) and Z-Phe-PNP ( $3.5 \times 10^{-5}$  M) in  $2C_{16}N^+2C_1$  ( $3.5 \times 10^{-4}$  M). Conditions: pH 7.2, 40 °C, 0.01 M Tris,  $\mu = 0.01$  (KCl).

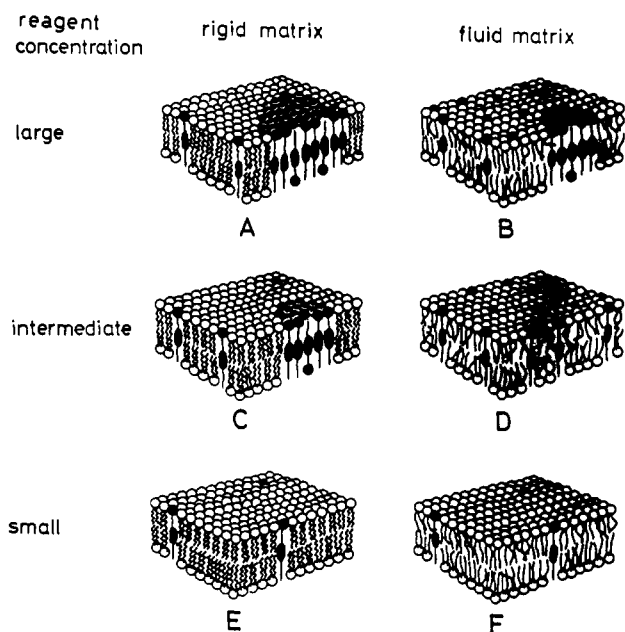


**Figure 11.** Schematic illustrations of the mode of reagent distribution in the crystalline and liquid-crystalline bilayer matrix.

coincides with  $\text{Cu}^{2+}$ -assisted phase separation. It is reported that the chelate formation can accelerate the hydrolysis.<sup>29,30</sup> However, this does not hold true in the present case, and  $\text{Cu}^{2+}$  only lowers the catalytic rate via the change of the membrane physical state.

#### Concluding Remarks

The membrane physical state is directly related to functions of the synthetic bilayer systems. It has been reported from these laboratories that inflection regions are noted in the Arrhenius plots of acyl transfer,<sup>31</sup> proton abstraction,<sup>32</sup> decarboxylation,<sup>33</sup> and

nucleophilic cleavage of phosphate esters<sup>34</sup> that proceed in the dialkylammonium membrane matrix. These inflections are usually present at or near the phase transition temperature of the matrix membrane, and the apparent activation energies are greater at temperatures below  $T_c$  than above  $T_c$ . These results certainly point to the importance of the fluidity of the membrane matrix in controlling reaction rates; however, it was not clear in the past studies why the membrane fluidity should affect the reaction rate. The present investigation provides at least a partial answer to this question. It is now established that the distribution of membrane-forming reagents (substrate and catalyst) in the bilayer matrix is highly dependent of the membrane physical state (crystalline or liquid crystalline). This factor should have been influential in reactions that involve hydrophobic reagents such as mentioned above, although we did not have means to determine the reagent distribution in those cases. The azobenzene amphiphile is a superior reagent in this respect, since its mode of aggregation (eg., cluster formation) in the membrane can be readily inferred by absorption spectroscopy. The cluster formation depends mainly on the molar ratio (two-dimensional concentration) of a reagent in the bilayer matrix and on the physical state of the matrix membrane. The nature of the head group is an additional factor. These situations are illustrated in Figure 11. When the reagent concentration is large, large clusters are formed in the rigid bilayer matrix (A). As the matrix becomes fluid, the cluster size (and number) decreases and the monomeric species increases (B). In the intermediate reagent concentration, the cluster is formed in the rigid matrix (C) but not in the fluid matrix (D). At small concentrations, the cluster is not formed in the rigid matrix (E) or in the fluid matrix (F). We examined the reactivity change due to formation of the bilayer cluster of a phenyl ester substrate and the activity change of the histidine catalyst due to formation of bilayer clusters. We have now at hand means to control the reactivities of both catalyst and substrate via the physical-state change. The principle of reaction control obtained in these systems should be applicable to other reactions.

(29) Buckingham, D. A.; Marzilli, L. G.; Sargeson, A. *J. Am. Chem. Soc.* **1967**, *89*, 2772-2773, 4539-4540.

(30) Ohkubo, K.; Arima, H.; Yoshinaga, K. *Inorg. Nucl. Chem. Lett.* **1978**, *14*, 287-290.

(31) Kunitake, T.; Sakamoto, T. *Chem. Lett.* **1979**, 1059-1062.

(32) Okahata, Y.; Tanamachi, T.; Kunitake, T. *Nippon Kagaku Kaishi* **1980**, 442-449.

(33) Kunitake, T.; Okahata, Y.; Ando, R.; Shinkai, S.; Hirakawa, S. *J. Am. Chem. Soc.* **1980**, *102*, 7877-7881.

(34) Okahata, Y.; Ihara, H.; Kunitake, T. *Bull. Chem. Soc. Jpn.* **1981**, *54*, 2072-2078.

## An Azocine Anion Radical and Heats of Formation of Azocine Dianions

Gerald R. Stevenson,\* Laurel E. Schock, Richard C. Reiter, and John F. Hansen

Contribution from the Department of Chemistry, Illinois State University, Normal, Illinois 61761. Received February 4, 1983

**Abstract:** 3,8-Dimethyl-2-methoxyazocine was reduced to its anion radical in hexamethylphosphoramide (HMPA). The ESR spectrum of the DMMA anion radical resembles one recorded from a monosubstituted cyclooctatetraene anion radical where the substituent is an electron-withdrawing group. Calorimetric techniques were utilized to study the thermodynamic stability of the DMMA dianion. This dianion is more stable relative to the metal and neutral molecule than is either the cyclooctatetraene (COT) or *tert*-butoxycyclooctatetraene dianion. The unexpected stability of  $\text{DMMA}^{2-}$  is attributed to strong interactions between the cation ( $\text{Na}^+$ ) with the oxygen and/or nitrogen atoms. This same interaction shifts the disproportionation of  $\text{DMMA}^{\cdot-}$  to the right in solvents where ion association is prevalent.

Like COT, the azocines undergo a two-electron reduction to give planar dianions that are aromatic in nature.<sup>1</sup> Using CV studies, 3,8-dimethyl-2-methoxyazocine (DMMA) undergoes a two-electron addition at about 2.5 V (it varies a little with the

choice of solvent). The behavior is consistent with the reduction of DMMA directly to the aromatic dianion (reaction 1).<sup>1</sup> A surprising result in this study (Paquette and co-workers<sup>1</sup>) is the fact that at the polarographic half-wave potential, the DMMA radical anion is easier to reduce than is the parent molecule, and the anion radical has never been observed. In fact, Paquette and co-workers have mentioned that the anion radical, if it does exist

(1) Anderson, L. B.; Hansen, J. F.; Kakihana, T.; Paquette, L. A. *J. Am. Chem. Soc.*, **1971**, *93*, 161.